J|A|C|S
ARTICLES
Published on Web 02/20/2002

Field-Dependent Electrode−Chemisorbate Bonding: Sensitivity of Vibrational Stark Effect and Binding Energetics to Nature of Surface Coordination

Sally A. Wasileski,[†] Marc T. M. Koper,[‡] and Michael J. Weaver,*[,†]

Contribution from the Department of Chemistry, Purdue University, West Lafayette, Indiana 47907, and Laboratory for Inorganic Chemistry and Catalysis, Schuit Institute of Catalysis, Eindhoven University of Technology, 5600 MB Eindhoven, The Netherlands

Received September 19, 2001. Revised Manuscript Received December 3, 2001

Abstract: Illustrative quantum-chemical calculations for selected atomic and molecular chemisorbates on Pt(111) (modeled as a finite cluster) are undertaken as a function of external field, F, by using Density Functional Theory (DFT) with the aim of ascertaining the sensitivity of the field-dependent metal−adsorbate binding energetics and vibrational frequencies (i.e., the vibrational Stark effect) to the nature of the surface coordination in electrochemical systems. The adsorbates selected − Cl, I, O, N, Na, NH_3, and CO − include chemically important examples featuring both electron-withdrawing and -donating characteristics. The direction of metal−adsorbate charge polarization, characterized by the static dipole moment, μ_S, determines the binding energy−field (E_b-F) slopes, while the corresponding Stark-tuning behavior is controlled primarily by the dynamic dipole moment, μ_D. Significantly, analysis of the F-dependent sensitivity of μ_S and μ_D leads to a general adsorbate classification. For electronegative adsorbates, such as O and Cl, both μ_S and μ_D are negative, the opposite being the case for electropositive adsorbates. However, for systems forming dative-covalent rather than ionic bonds, as exemplified here by NH_3 and CO, μ_S and μ_D have *opposite* signs. The latter behavior, including electron-donating and -withdrawing categories, arises from diminishing metal−chemisorbate orbital overlap, and hence the extent of charge polarization, as the bond is stretched. A clear-cut distinction between these different types of surface bonding is therefore obtainable by combining vibrational Stark-tuning and E_b-F slopes, as extracted from experimental data and/or DFT calculations. The former behavior is illustrated by means of potential-dependent Raman spectral data obtained in our laboratory.

Introduction

The energetics of chemisorbate binding at metal−solution interfaces are well known to be sensitive to the applied electrode potential and hence the local electrostatic field. Understanding the fundamental bonding interactions responsible, however, has been limited somewhat by the paucity of microscopic-level techniques, at least in comparison with the situation for metal surfaces in ultrahigh vacuum (UHV). Nevertheless, aside from thermodynamic-based information on metal−adsorbate adsorption energies, in-situ vibrational spectroscopy can provide microscopic-level information into electrode−chemisorbate bonding.[1] In particular, one anticipates that examining the dependence of chemisorbate vibrational frequencies on the electrode potential and hence the local electrostatic field, i.e., the electrochemical Stark effect,[2] should yield important insight regarding charge polarization.

Following earlier ab initio[3,4] and semiempirical calculations,[5] the recent emergence of Density Functional Theory (DFT) as a reliable quantum-chemical means of describing metal surface−chemisorbate bonding is having an important impact on our interpretation of such vibrational as well as other energetic properties. While slab-based DFT calculations can yield more accurate binding energetics for higher adsorbate coverages at uncharged metal surfaces, related studies for single adsorbates on finite metal clusters bathed in variable external fields provide a useful semiquantitative way of mimicking the adjustable surface potential in electrochemical systems. A number of recent DFT calculations of the latter type have been concerned with understanding such field-dependent vibrational properties.[4−10] Our initial investigations along these lines concerned carbon monoxide and nitric oxide on (111) surfaces of platinum-group

* Corresponding author. E-mail: mweaver@purdue.edu.
[†] Purdue University.
[‡] Eindhoven University of Technology.

(1) For a review, see Weaver, M. J.; Zou, S. In *Spectroscopy for Surface Science*; Advances in Spectroscopy, Vol. 26; Clark, R. J. H., Hester, R. E., Eds.; Wiley: Chichester, U.K., 1998; Chapter 5.
(2) For an overview, see Lambert, D. K. *Electrochim. Acta* **1996**, *41*, 623.
(3) For example: Bagus, P. S.; Pacchioni, G. *Electrochim. Acta* **1991**, *36*, 1669.
(4) Head-Gordon, H.; Tully, J. C. *Chem. Phys.* **1993**, *175*, 37.
(5) Anderson, A. B. *J. Electroanal. Chem.* **1990**, *280*, 37.
(6) (a) Illas, F.; Meli, F.; Curulla, D.; Clotet, A.; Ricart, J. M. *Electrochim. Acta*. **1999**, *44*, 1213. (b) Curulla, D.; Clotet, A.; Ricart, J. M.; Illas, F. *Electrochim. Acta* **1999**, *45*, 1999. (c) Garcia-Hernandez, M.; Curulla, D.; Clotet, A.; Illas, F. *J. Chem. Phys*. **2000**, *113*, 364.
(7) (a) Liao, M.-S.; Zhang, Q.-E. *J. Chem. Soc., Faraday Trans*. **1998**, *94*, 1301. (b) Liao, M.-S.; Cabrera, C. R.; Ishikawa, Y. *Surf. Sci*. **2000**, *445*, 267.
(8) Koper, M. T. M.; van Santen, R. A. *J. Electroanal. Chem*. **1999**, *476*, 64.

10.1021/ja012200w CCC: $22.00

metals (Pt, Ir, Pd, Rh, and Ru),[8,9] motivated partly by the extensive experimental information now available for the potential-dependent intramolecular infrared vibrations for electrochemical CO and NO adlayers.[11] Also of particular fundamental interest are the field-dependent vibrational frequencies of the metal−adsorbate bond itself, ν_{M-A}. While largely inaccessible to surface infrared spectroscopy, such low-frequency modes can readily be detected at electrochemical interfaces by surface-enhanced Raman spectroscopy (SERS): significantly, the available SERS-active surfaces include Pt-group metals by employing thin overlayer films on gold substrates.[12] This capability has enabled us to explore the potential-dependent ν_{M-A} behavior for halogens and other monoatomic adsorbates[13] as well as ν_{M-A} and intramolecular vibrations for a range of polyatomic species.[14−16]

The availability of such electrochemical vibrational data has encouraged us to utilize DFT calculations as a means not only of furnishing a more complete interpretation in terms of surface chemical bonding, but also to explore the relationships between field-dependent vibrational frequencies, surface−chemisorbate binding energies, and bond geometries. The central significance of establishing such relationships, of course, lies in the desire to utilize DFT-based calculations so as to forge a more complete understanding of the surface vibrational data in terms of quantum chemistry. An initial finite-cluster DFT investigation for CO chemisorbed on Pt-group surfaces showed a close connection only between ν_{M-A} and bond lengths, although a decomposition into metal−CO donation and back-donation components indicated the importance of both interactions in the field-dependent bond energy and ν_{M-A} behavior.[9c] Most recently, we have outlined a general treatment of such field-dependent parameters in terms of surface bond polarization, specifically static (μ_S) and dynamic dipole moments (μ_D), and exemplified by means of illustrative DFT calculations for simple monatomic adsorbates.[10] Essentially, the field- (F-) dependent binding energy (E_b) is determined by μ_S , whereas the Stark-tuning ($\nu_{M-A}-F$) behavior is controlled primarily by μ_D along with bond anharmonicity.[10]

This quantitative recognition of the central roles played by charge polarization in electrode-surface bonding suggested that the binding energy and vibrational parameters should be sensitive to, and thereby could shed light on, the fundamental nature of the surface coordination. That is, one would anticipate that the type of metal−adsorbate interactions, such as the direction and extent of charge polarization, the involvement of σ and π orbitals, and so on, should be reflected − perhaps differently − in the field-dependent binding energy and Stark-tuning behavior in a fashion that enables their identification and diagnosis.

Intriguingly, this expectation turns out largely to be correct. The present paper contains illustrative DFT calculations, specifically for monoatomic adsorbates (Cl, I, O, N, Na) forming surface bonds with widely varying polarity and for simple molecular adsorbates (CO, NH_3) having distinctly differing orbital interactions, with the overall aim of forging such a connection between the bond polarization parameters and the nature of surface coordination. Broadly speaking, the analysis identifies three distinct classes of metal−chemisorbate coordination, based on the relative signs of the μ_S and μ_D values, and hence differing E_b-F relative to $\nu_{M-A}-F$ behavior. Overall, the DFT results (together with salient experimental data) point to the general utility of the analysis for exploring the nature of electrode−adsorbate coordination.

Computational Methods

The DFT calculational procedures followed those described in refs 9 and 10. Most calculations utilized a neutral atomic or molecular adsorbate bound to a 13-atom C_{3v} platinum (111) cluster, arranged in two hexagonal layers of six and seven atoms each. (Although larger clusters were also utilized,[9] this M_{13} geometry was deemed sufficient for the present illustrative purposes.) The metal interatomic distance was fixed at the experimental bulk-phase value of 2.775 Å. The adsorbates were arranged centrally on the seven- and six-atom layers in atop (1-fold) and 3-fold hollow sites, respectively, the molecular species being bound such that the molecular axis of symmetry is perpendicular to the surface plane so to maintain C_{3v} symmetry. The ammonia adsorbate was oriented such that the N−H bonds were staggered between the metal atoms on the surface plane, with the intramolecular bond distances and angles relaxed to their equilibrium values at $F = 0$ and held fixed for simplicity. (The intramolecular geometry changes only slightly upon adsorption.[16]) The intramolecular bond distance for coordinated CO, however, was relaxed to its equilibrium position at each applied field, as it changes significantly.[9c] As usual,[6−9] variable homogeneous external fields, F, were applied along the cluster C_{3v} axis.

The calculations utilized the Amsterdam Density Functional Package (ADF 2000.03, Department of Theoretical Chemistry, Vrije Universiteit, Amsterdam).[17] Slater-type functions are used to represent atomic orbitals. To enhance computational efficiency, the innermost atomic shells are kept frozen up to the following orbitals: Na 1s, C 1s, N 1s, O 1s, Cl 2p, I 4p, and Pt 5p. All basis sets are of double-ζ quality, while the H, Na, C, N, O, and Cl basis sets are augmented by polarization functions. The Kohn−Sham one-electron equations were solved in the DFT-GGA approximation. The Vosko−Wilk−Nusair form of the local density approximation[18] was used in combination with the BP86 functional for the generalized gradient approximation (GGA).[19] Even though significantly different metal−adsorbate binding energies are obtained with other functionals, such as PW91 and BLYP, the dependence of this quantity as well as force constants on the external field, of primary interest here, is insensitive to the choice of functional. Relativistic effects within the cores were accounted for self-consistently by first-order perturbation theory. Cluster and isolated molecule

(9) (a) Koper, M. T. M.; van Santen, R. A.; Wasileski, S. A.; Weaver, M. J. *J. Chem. Phys.* **2000**, *113*, 4392. (b) Wasileski, S. A.; Weaver, M. J.; Koper, M. T. M. *J. Electroanal. Chem.* **2001**, *500*, 244. (c) Wasileski, S. A.; Koper, M. T. M.; Weaver, M. J, *J. Phys. Chem. B* **2001**, *105*, 3518.
(10) Wasileski, S. A.; Koper, M. T. M.; Weaver, M. J. *J. Chem. Phys.* **2001**, *115*, 8193.
(11) For recent discussions, see (a) Weaver, M. J.; Zou, S.; Tang, C. *J. Chem. Phys.* **1999**, *111*, 368. (b) Weaver, M. J. *Surf. Sci.* **1999**, *437*, 215. (c) Weaver, M. J.; Wasileski, S. A. *Langmuir* **2001**, *17*, 3039.
(12) For an overview, see Weaver, M. J.; Zou, S.; Chan, H. Y. H. *Anal. Chem.* **2000**, *72*, 38A.
(13) (a) Mrozek, M. F.; Weaver, M. J. *J. Am. Chem. Soc.* **2000**, *122*, 150. (b) Gao, P.; Weaver, M. J. *J. Phys. Chem.* **1986**, *90*, 4057.
(14) (a) Zou, S.; Weaver, M. J. *J. Phys. Chem.* **1996**, *100*, 4237. (b) Zou, S.; Gómez, R.; Weaver, M. J. *Langmuir* **1997**, *13*, 6713.
(15) For example, see (a) Mrozek, M. F.; Weaver, M. J. *J. Phys. Chem. B* **2001**, *105*, 8931. (b) Mrozek, M. F.; Wasileski, S. A.; Weaver, M. J. *J. Am. Chem. Soc.* **2001**, *123*, 12817. (c) de Vooys, A. C. A.; Mrozek, M. F.; Koper, M. T. M.; van Santen, R. A.; van Veen, J. A. R.; Weaver, M. J. *Electrochem. Comm.* **2001**, *3*, 293.
(16) (a) Illas, F.; López, N.; García-Hernández, M.; Moreira, I. de P. R. *J. Mol. Struct.* **1999**, *458*, 93. (b) García-Hernández, M.; López, N.; Moreira, I. de P. R.; Paniagua, J. C.; Illas, F. *Surf. Sci.* **1999**, *430*, 18.
(17) (a) Amsterdam Density Functional Package, ADF 2000.03, Department of Theoretical Chemistry, Vrije Universiteit, Amsterdam, 2000. (b) Baerends, E. J.; Ellis, D. E.; Ros, P. *Chem. Phys.* **1973**, *2*, 41. (c) Versluis, L.; Ziegler, T. *J. Chem. Phys.* **1988**, *88*, 322. (d) te Velde, G.; Baerends, E. J. *J. Comput. Phys.* **1992**, *99*, 84. (e) Fonseca-Guerra, C.; Snijders, J. G.; te Velde, G.; Baerends, E. J. *Theor. Chem. Acc.* **1998**, *99*, 391.
(18) Vosko, S. H.; Wilk, L.; Nusair, M. *Can. J. Phys.* **1980**, *58*, 1200.
(19) (a) Becke, A. D. *Phys. Rev. A* **1988**, *38*, 3098. (b) Lee, C.; Yang, W.; Parr, P. G. *Phys. Rev. B* **1988**, *37*, 785.

calculations were undertaken in the spin-restricted mode, and all isolated atom calculations were spin-unrestricted.

The binding energy for each metal−adsorbate bond distance, r_{M-A}, was determined by subtracting the total energy (from the standard ADF output) for the isolated adsorbate and bare cluster from those for the ligated cluster, with the external field applied across the cluster, but not the unbound adsorbate. The corresponding surface−adsorbate dipole moments were obtained from the total value for the ligated cluster minus the value for the bare cluster at the same field. Potential-energy surfaces and dipole moment−r_{M-A} curves were obtained from calculations for 9−11 r_{M-A} values encompassing ±0.2 to ±0.4 Å from equilibrium. The relatively wide range of r_{M-A} values chosen ensures that the potential-energy surface includes anharmonic contributions (vide infra). (All r_{M-A} values given here are the perpendicular center-to-center distance from the top-layer metal atoms to the adsorbate lead-in atom.)

Results and Discussion

Trends in Field-Dependent Surface Dipole Moments: Relation to Binding Energetics and Vibrational Frequencies. As a starting point, it is appropriate to summarize the relationships (detailed in ref 10) linking the surface dipole-moment parameters, of central interest here, with the field-dependent binding energies and vibrational frequencies, of primary experimental relevance. The surface−adsorbate dipole moment can conveniently be expressed as a function of the bond distance, r_{M-A}, at a given external field F as

$$\mu(q) = \mu_S + \mu_D q + a_D q^2 \quad (1)$$

where $q = 0$ refers to the equilibrium bond distance, corresponding to the so-called "static" dipole moment μ_S. Bond displacements away from equilibrium (i.e., $q \neq 0$), of central interest in vibrational spectroscopy, are described (for small $|q|$) in terms of the $\mu-q$ tangent, or "dynamic dipole moment", μ_D, along with the second-order term a_D in eq 1.

For the most part, μ_S and μ_D describe the dependence of the metal−adsorbate binding energy, E_b, and vibrational parameters, respectively, on the external field and hence the electrode potential in electrochemical systems.[10] The former relationship is simply[10,20]

$$\mu_S = -(dE_b/dF) \quad (2)$$

provided that the influence of higher-order multipoles can be neglected (vide infra).[10] The corresponding relationship linking μ_D to the potential-energy surface (PES) for small q displacements can from eqs 1 and 2 be written as

$$\mu_D = -(\partial^2 E/\partial F \partial q)_F \quad (3)$$

The PES is described conventionally in polynomial form as

$$E = E_b + (1/2)Kq^2 + Gq^3 \quad (4)$$

where K is the vibrational force constant and G is the anharmonicity parameter. A particularly useful relation, derived from the above, expresses the force constant−field slope at a given F as[10,21]

$$\left(\frac{dK}{dF}\right)_F = \frac{6G\mu_D - 2Ka_D}{K} \quad (5)$$

As we shall see below, the "Stark-tuning" slope is often determined primarily by the $(G/K)\mu_D$ term rather than a_D.[10] Examining the sensitivity of both μ_S and μ_D to the nature of the surface bonding, as determined here by DFT, is therefore expected to provide substantial insight into the field-dependent nature of the PES.

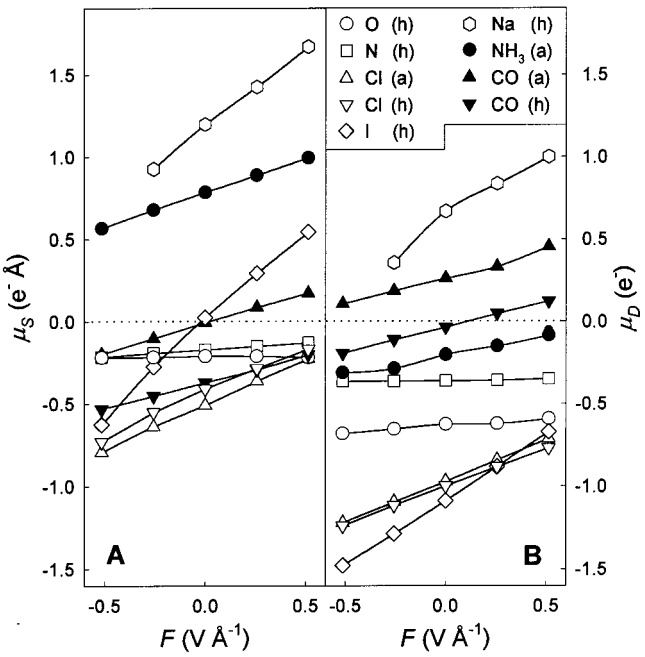

Figure 1. (A) Plot of static dipole moment μ_S (i.e., at equilibrium bond distance) as deduced from DFT for various chemisorbates as indicated, on hollow (h) and atop (a) sites on Pt(111) versus applied external field. (B) Same as for panel A but for dynamic dipole moment μ_D at equilibrium bond distance.

Panels A and B of Figure 1 show plots of μ_S and μ_D, respectively, versus F for a representative selection of atomic and molecular chemisorbates on Pt(111), modeled as noted above as a Pt_{13} cluster. (Although selecting other cluster sizes and geometries led to significantly different μ_S and μ_D values in some cases, the results are adequate for the present illustrative purposes.) Platinum was selected for consideration here as the archetypical Pt-group metal, having broad-based significance in chemisorption and catalysis. The range of fields in Figure 1, from ca. −0.5 to 0.5 V $Å^{-1}$, encompasses the values normally encountered in electrochemical systems. As discussed earlier,[9c,33] this corresponds to a range of electrode potentials from roughly −1.5 to 1.5 V relative to an uncharged surface, the precise values being dependent on the inner-layer thickness.

The choice of adsorbates included in Figure 1 was prompted by several factors. Atomic oxygen and chlorine constitute typical electronegative adsorbates, thereby forming highly polar bonds, and iodine is included as an example of a more polarizable atomic adsorbate. Although chemisorbed sodium is not usually observable in electrochemical systems due to solvation, it is included to represent the behavior of a strongly electropositive

(20) (a) Mortensen, J. J.; Hammer, B.; Nørskov, J. K. *Surf. Sci.* **1998**, *414*, 315. (b) Nørskov, J. K.; Holloway, S.; Land, N. S. *Surf. Sci.* **1984**, *137*, 65.

(21) (a) Lambert, D. K. *Solid State Commun.* **1984**, *51*, 297. (b) Lambert, D. K. *J. Chem. Phys.* **1988**, *89*, 3847.

atom. The molecular adsorbates NH_3 and CO, aside from their experimental chemical importance, were selected as species that bind via electron donation and partial back-donation, respectively. The final adsorbate chosen, atomic nitrogen, offers a useful comparison to ammonia. Dipole-moment data are given in Figure 1 for all atomic adsorbates in a 3-fold-hollow site, since this provides the experimentally (and computationally) most favorable binding geometry, although data for atop-bound chlorine are also shown. Results for both atop and hollow-site CO are included, since both binding modes are encountered experimentally,[9] and the degree of bond polarization (as reflected in the μ_S and μ_D values) for the bonding geometries is quite distinct. Finally, only data for atop NH_3 are included for clarity, since the corresponding results for hollow-site NH_3 are closely similar.

Careful inspection of the μ_S−F data in Figure 1A reveals several significant features. First, as might be expected, the μ_S values at $F = 0$ roughly correlate with the anticipated electron-donating/withdrawing ability of the different adsorbates. Thus the electronegative atoms oxygen and chlorine both yield negative μ_S values, implying metal−adsorbate electron withdrawal, even though the greater negative μ_S value for the latter presumably reflects its larger size. The markedly more negative μ_S value for hollow-site versus atop CO is consistent with the greater extent of back-donation expected for the former binding geometry.[9] The large positive μ_S value for adsorbed NH_3 reflects chiefly ammonia−metal electron donation. By and large, these trends in μ_S at $F = 0$, calculated from DFT, are consistent with estimates extracted from work function−adsorbate coverage data obtained at the Pt(111)−UHV interface. These latter "experimental" values, μ_S(exp), where available, are tabulated alongside the corresponding DFT estimates at $F = 0$, μ_S(DFT), in Table 1. [Note that the units of μ_S used here are e^- Å, where 1 D ≡ 0.21 e^- Å. The formula used to extract these μ_S(exp) values is noted in footnote 22, with data sources given in the footnotes to Table 1.] Also included in Table 1 (in parentheses) are the μ_S(DFT) and μ_S(exp) values for the unbound molecular adsorbates, taken along the same direction as the metal−adsorbate bond axis. While these latter values are very small for CO, indicating that the chemisorbate dipole results almost entirely from surface bond formation, the polar molecule NH_3 exhibits a significant uncoordinated dipole (0.3 e^- Å), so that the large positive μ_S values for adsorbed NH_3 probably arise partly from an "intrinsic intramolecular" contribution.

Another interesting aspect of the results in Figure 1A concerns the μ_S−F slopes, which can be identified with the polarizability tensor of the metal−adsorbate bond, α_z, along the field direction, normal to the surface. Such DFT-deduced polarizability values (for $F \rightarrow 0$), expressed (as is conventional[30]) as polarizability volumes (Å^3), $\alpha'_z = \alpha_z/4\pi\epsilon_0$ (ϵ_0 is the permittivity of free space), are also given for each adsorbate in Table 1, labeled α'_z(M-A). Listed alongside in the far right-hand column are the corresponding α'_z values for the *uncoordinated* adsorbate, α'_z(A), taken (or estimated) from the literature (see table footnotes). As might be expected, the α'_z(M-A) values are larger than the corresponding α'_z(A) quantities (with the exception of Pt−O), reflecting the additional polarizability generated by the metal surface bond. Interestingly, the former values tend to vary with the adsorbate in a fashion similar to the latter, so that in most cases roughly α'_z(M-A) ∼ 2−4 times α'_z(A). This finding suggests that the free adsorbate polarizability plays an important role in determining the behavior of the metal−adsorbate adduct.

An important consequence of the relatively large as well as chemisorbate-sensitive values of α'_z(M−A) is that applying positive or negative fields can alter μ_S substantially, even changing sign in some cases (Figure 1A). For example, the polarizable adsorbate iodine can attain substantial negative or similarly positive μ_S values over the range of fields shown in Figure 1A, whereas the smaller "nonpolarizable" oxygen or nitrogen chemisorbates yield largely field-invariant and negative μ_S values. Atop CO is another example where μ_S changes sign with varying field, arising in this case from alterations in the degree of metal−CO σ donation and π back-donation (vide infra). The overall consequence of these trends is that the magnitude and even sign of the binding energy−field depen-

Table 1. Static Dipole and Polarizability Parameters at $F = 0$

adsorbate (Pt_{13})	μ_s(DFT) [a] (e^-Å)	μ_s(exp) [b] (e^-Å)	α'_z(M-A) [c] (Å^3)	α'_z(A) [d] (Å^3)
O (h)	−0.21	−0.06[e]	<0.1	0.43
N (h)	−0.17		1.2	0.45
Cl (a)	−0.51		7.9	1.75
Cl (h)	−0.41	<−0.1[f]	7.8	1.75
I (h)	0.03		16.3	4.3
Na (h)	1.2	1.4[g]	14.0	11.5
NH_3 (a)	0.78 (0.31)		6.0	2.4
NH_3 (h)	0.70 (0.31)	0.8[h] (0.31)	7.0	2.4
CO (a)	0.004 (≈0.00)	0.15[i] (0.02)	5.2	2.3
CO (h)	−0.37 (≈0.00)		4.6	2.3

[a] Static dipole moment estimated from DFT at $F = 0$. Values given in parentheses for the molecular adsorbates are for the uncoordinated species aligned in the same direction, also determined from DFT. (Note that 1 D ≡ 0.21 e^-Å.) [b] Static dipole moment estimated (at $F = 0$) from work function−coverage data at Pt(111)−UHV interfaces, as obtained in footnote 22, from references noted. Values given in parentheses are experimental dipole moments for the free molecules along the same direction as the metal−adsorbate bond, from tabulation in ref 32. [c] Polarizability tensor values for Pt_{13}−adsorbate system, obtained from DFT μ_s−F data (Figure 1A) as noted in text. [d] Polarizability tensor volume (along direction of surface bond axis z) for uncoordinated adsorbate, extracted chiefly from compilation in ref 31; values for atomic adsorbates were estimated from polarizabilities of adjacent noble-gas atoms, with adjustment for differing atomic size (and hence volume). [e] Reference 24. [f] References 25 and 26. [g] Reference 27. [h] Reference 28. [i] Reference 29.

(22) The "experimental" dipole moments in Table 1 were determined numerically from[23] μ_S(exp) (in Debyes) = (-5.31×10^{14})dΦ/dn, where the initial slope of the work function (Φ) versus adsorbate density (n) plot, dΦ/dn, is expressed in eV mol^{-1} cm^2. (Note that 1 D ≡ 0.21 e^- Å, as employed here.) However, there is some ambiguity in the choice of numerical coefficient in the above formula: if the surface point dipole is defined in terms of adatom effective charge separated from the outmost metal atomic layer rather than the image plane in the metal, 2-fold smaller μ_S(exp) values are obtained.[23b] This complication, however, is unimportant for the present limited purposes.

(23) For example: (a) Hölzl, J.; Schutle, F. K. In *Springer Tracts in Modern Physics*; Holher, G., Niekisch, E. A., Eds.; Springer: Berlin, 1979; Vol. 85, p 1. (b) Wandelt, K. In *Physics and Chemistry of Alkali Metal Adsorption*; Bonzel, H. P., Bradshaw, A. M., Ertl, G., Eds.; Elsevier: Amsterdam, 1989; p 25.
(24) Parker, D. H.; Bartram, M. E.; Koel, B. E. *Surf. Sci.* **1989**, *217*, 489.
(25) Villegas, I.; Weaver, M. J. *J. Phys. Chem.* **1996**, *100*, 19502.
(26) Wasileski, S. A.; Weaver, M. J. *J. Phys. Chem. B* (in press).
(27) Bonzel, H. P.; Pirug, G.; Ritke, C. *Langmuir* **1991**, *7*, 3006.
(28) (a) Fisher, G. B. *Chem. Phys. Lett.* **1981**, *79*, 452. (b) Villegas, I.; Weaver, M. J. *Surf. Sci.* **1996**, *367*, 162.
(29) Poelsema, P.; Palmer, R. L.; Comsa, G. *Surf. Sci.* **1982**, *123*, 152.
(30) For example, see Atkins, P. *Physical Chemistry*, 6th ed.; Freeman: New York, 1997; p 653.
(31) From polarizability tensor tabulation in Böttcher, C. J. F.; Bordewijk, P. *Theory of Electric Polarization*, 2nd ed.; Elsevier: Amsterdam, 1978; Vol. 2, p 332.
(32) (a) McClennin, A. L. *Tables of Experimental Dipole Moments*; W. H. Freeman: San Francisco, CA, 1963. (b) For carbon monoxide, see also Billingsley, F. P.; Krauss, M. *J. Chem. Phys.* **1974**, *60*, 4130.
(33) Weaver, M. J. *Appl. Surf. Sci.* **1993**, *67*, 147.

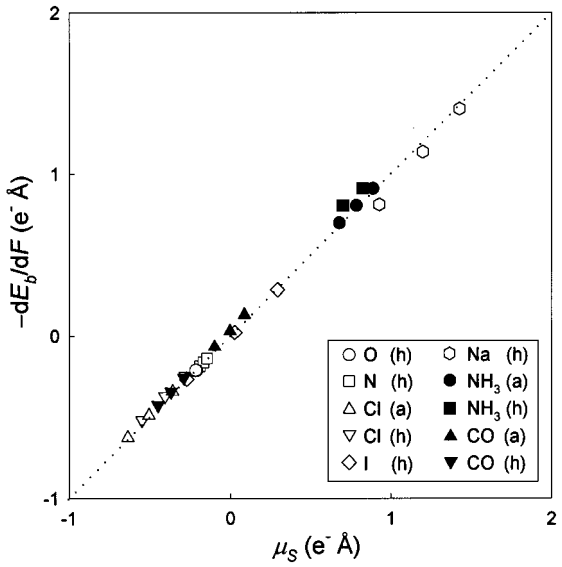

Figure 2. Test of the applicability of eq 2 for the present Pt(111)−adsorbate systems, as indicated, over the range of fields (−0.5 to 0.5 V Å^{-1}) considered here.

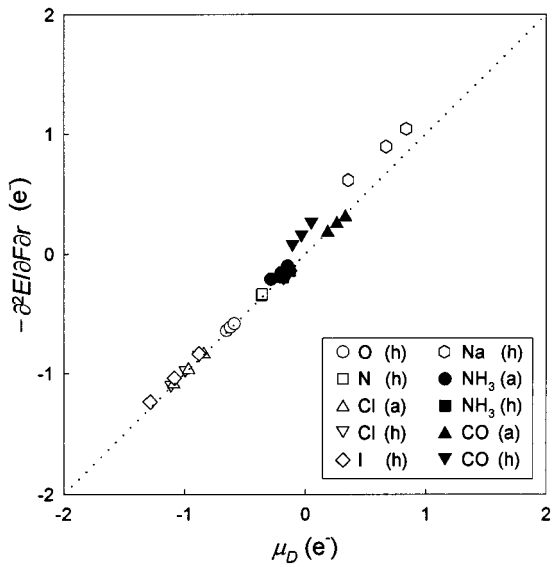

Figure 3. Test of the applicability of eq 3 for the present Pt(111)−adsorbate systems, as indicated, over the range of fields (−0.5 to 0.5 V Å^{-1}) considered here.

dence derived from the μ_S values, as prescribed by eq 2, can be sensitive to the value of the applied field as well as the nature of the adsorbate.

Turning now to the corresponding dynamic dipole moment−field (μ_D−F) plots in Figure 1B, some trends in the adsorbate-dependent μ_D behavior are reminiscent of those seen for the μ_S values. Thus the strongly electronegative adsorbates oxygen, nitrogen, and chlorine exhibit negative μ_D as well as μ_S values at all fields, as expected since the partial negative charge residing on the adsorbate is retained as r_{M-A} is lengthened. However, the behavior of adsorbed iodine is quite different, large negative μ_D values being obtained at all fields (Figure 1B), contrasting with the μ_S sign reversal seen at positive versus negative fields (Figure 1A). The molecular adsorbates also show distinctly different μ_S and μ_D trends, most noticeably ammonia, which exhibits negative μ_D yet positive μ_S values at all fields. As we shall see below, such behavioral differences between μ_S and μ_D have important ramifications for understanding the nature of surface coordination.

Given the predicted importance of μ_S and μ_D in determining the field dependence of the metal−adsorbate binding energy and the PES, as prescribed by eqs 2 and 3, respectively, it is important to check the applicability of these relationships, especially since their derivation requires the neglect of higher-order multipoles (vide supra). Figure 2 plots dE_b/dF for the adsorbate systems considered here on Pt(111) over a range of selected fields (similar to that in Figure 1) versus μ_S, the bond energy and dipole moments being calculated *separately* by DFT. The quantitative applicability of eq 2 is evident from the close concordance between the points and the unit slope/zero intercept dotted line, the deviations typically being less than 5%. Figure 3 is a corresponding check on the validity of eq 3, i.e., a plot of $\partial^2 E/\partial F \partial q$ versus μ_D for the same systems and conditions as in Figure 2. Again a reasonable concordance is evident, although significant systematic deviations are seen for hollow-site CO and sodium (Figure 3).

Chemisorbate Bonding Classification in Terms of Field-Dependent Dipole Parameters. Having confirmed this intimate link between the μ_S and μ_D values in Figure 1 with the field-dependent binding energy and Stark-tuning behavior, it is instructive to undertake a classification of the adsorbate dipole parameters with the aim of ascertaining broad-based connections between the former experimentally accessible quantities and the modes of surface coordination. Significantly, careful scrutiny of Figure 1 enables three classes of chemisorbate bonds to be distinguished, depending on the *sign* of the static versus the dynamic dipole moment.

For the majority of the chemisorbates considered here, especially toward negative fields, both μ_S and μ_D have a negative sign. Representative members of this category, labeled here "Class A" (or "anion-like"), are the electronegative adsorbates O, N, and Cl. Such behavior, of course, is expected since the chemisorbed atom will carry a partial negative charge, producing a negative μ_S value, and the movement of this charge away from the surface when the metal−adsorbate bond is stretched will yield a progressively more negative dipole, and hence a μ_D value of the same sign. Indeed, the observation of large negative (or positive) μ_D values has been regarded previously as a diagnosis of ionic surface bonding.[34] Similarly, then, for strongly electropositive adsorbates, as represented here by Na, both μ_S and μ_D should be positive, as is indeed the case (Figure 1). We label this latter "cation-like" behavior "Class C". This dipole moment−bond distance (μ−r_{M-A}) behavior characteristic of ionic bonding, either Class A or C, is exemplified at $F = 0$ for the specific examples Pt/Cl and Pt/Na in the left-hand portion of Figure 4. [The range of r_{M-A} values shown is ca. ±0.2−0.4 Å from equilibrium, as denoted by the vertical arrow, to which μ_S refers. Also note that the μ−r_{M-A} plots are strictly nonlinear, i.e., the higher-order term $a_D \neq 0$ (vide infra).]

However, some adsorbates in Figure 1 exhibit μ_S and μ_D values having the *opposite* sign over a given range of fields;

(34) For example: (a) Pacchioni, G.; Bagus, P. S.; Philpott, M. R.; Nelin, C. J. *Int. J. Quantum Chem.* **1990**, *28*, 675. (b) Lang, N. D. *Surf. Sci.* **1994**, *299/300*, 284.

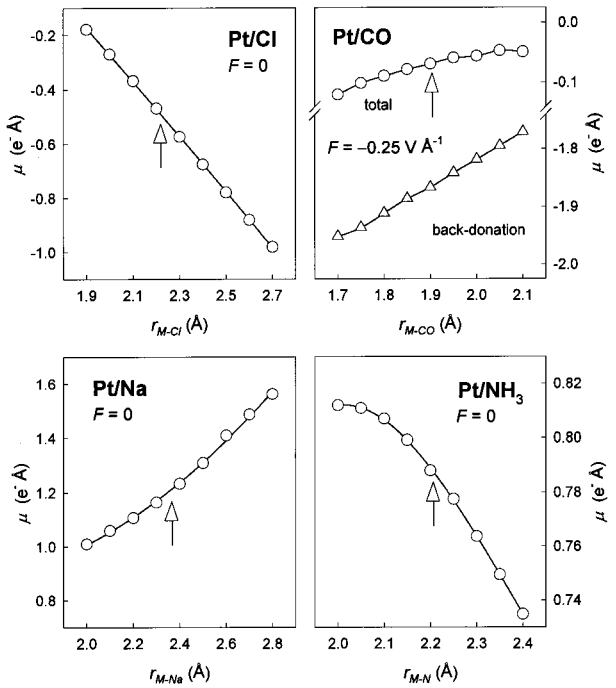

Figure 4. Plots of Pt(111)−adsorbate dipole moment, μ, versus bond distance, r_{M-A}, for four adsorbates (hollow site Cl and Na; atop CO and NH_3) of interest here, evaluated at $F = 0$, except for Pt/CO, which refers to $F = -0.25$ V Å^{-1}. Vertical arrows indicate equilibrium r_{M-A} values. Plot indicated with triangles for Pt/CO refers to dipolar component associated with (E symmetry) π back-donation (see text).

we designate these systems here as "Class B". The most clear-cut example is ammonia, which yields large positive μ_S values over the entire field range in Figure 1A, yet exhibits uniformly negative μ_D values. While a portion of the positive μ_S values may be attributed to an intramolecular contribution, as already mentioned, the markedly larger values seen for the chemisorbate (Figure 1A) indicate the importance of ammonia−metal electron donation.[35] Unlike electropositive adsorbates such as sodium, which also exhibit positive μ_S values, however, stretching the Pt−NH_3 bond yields a progressive *diminution* of the positive dipole moment due to weaker orbital overlap and hence a smaller extent of electron donation, thereby giving rise to *negative* $\mu-r_{M-A}$ slopes and hence μ_D values (Figure 1B). This point is graphically evident in the $\mu-r_{M-A}$ plots shown for the Pt/NH_3 and Pt/Na systems (at $F = 0$) in the lower portion of Figure 4: even though uniformly positive dipole moments are obtained in both cases, at least for r_{M-A} values close to equilibrium, the $\mu-r_{M-A}$ slopes (i.e., μ_D values) are qualitatively different.

In addition to ammonia, iodine adsorption at $F > 0$ yields the same combination of positive μ_S and negative μ_D values. Evidently, the degree of field-induced electron donation from the polarizable iodine atom, responsible for the positive μ_S values, is diminished steadily as r_{M-A} increases, leading to negative μ_D values. Note, however, that ammonia exhibits Class B behavior in the absence as well as in the presence of external fields of either sign, whereas iodine behaves in this fashion only for $F > 0$, yielding instead Class A characteristics when $F < 0$ (Figure 1). This suggests that a useful distinction might be drawn between "intrinsic" and "extrinsic" charge polarization behavior,

(35) Baetzold, R. Z.; Apai, G.; Shustorovich, E. *Appl. Surf. Sci.* **1984**, *19*, 135.

Table 2. Chemisorbate Dipole Classification

Class A ($-\mu_S/-\mu_D$)	Class B_w ($-\mu_S/+\mu_D$)	Class B_d ($+\mu_S/-\mu_D$)	Class C ($+\mu_S/+\mu_D$)
Cl, O, N	CO(a) ($F < 0$)	NH_3	Na
I ($F < 0$)	CO(h) ($F > 0$)	I ($F > 0$)	CO(a) ($F > 0$)
CO(h) ($F \lesssim 0$)			

the former referring only to $F = 0$ and the latter requiring the presence of external fields.

In addition to such behavior featuring electron donation, designated here more specifically as "Class B_d", one can envisage covalently bound adsorbates featuring primarily electron back-donation (or more generally electron withdrawal), where μ_S is thereby negative, yet again involving attenuation of orbital overlap as r_{M-A} increases, yielding positive μ_D values. This behavior, labeled here as "Class B_w", is exhibited by atop CO at $F < 0$, and hollow-site CO for $F > 0$ (Figure 1). A complication is that the metal−CO binding involves σ electron donation as well as π back-donation, yielding offsetting charge-polarization effects; these almost cancel for atop Pt/CO at $F = 0$, so that $\mu_S(F = 0) \approx 0$. Fortunately, the ADF−DFT calculations enable an approximate separation between these bonding modes to be achieved on symmetry grounds for the present metal clusters.[9] Plotted in the upper right-hand segment of Figure 4 are the contributions to the $\mu-r_{M-A}$ behavior associated only with π back-donation (along with the steric interactions), together with the total $\mu-r_{M-A}$ plot (i.e., including also σ donation) as before. At the negative field chosen ($F = -0.25$ V Å^{-1}), the total $\mu-r_{M-A}$ curve yields net negative μ_S and positive μ_D values (i.e., Class B_w behavior). Figure 4 also shows clearly that this results from the effects of back-donation outweighing the donation contribution.

Overall, then, one encounters four distinguishable types of bond length-dependent dipole-moment behavior, as exemplified (at $F = 0$) in the four $\mu-r_{M-A}$ plots shown in Figure 4, corresponding to Class A (Pt/Cl), Class C (Pt/Na), and Classes B_d and B_w (Pt/NH_3 and Pt/CO, respectively). A classification of each of the adsorbates (and field conditions) examined here is summarized in Table 2. The r_{M-A}-dependent nature of the surface coordination envisaged for these charge-polarization modes is illustrated in cartoon fashion in Figure 5 for the same four examples included in Figure 4. The degree of electron polarization to and from the chemisorbate atom/molecule for shorter and longer r_{M-A} values is designated by the arrow thickness (denoting the direction of charge transfer) together with the shading density within the adsorbate orbital lobes. In particular, the fundamental difference between "ionic" (Classes A and C) and "dative covalent" surface binding (Classes B_w and B_d) is clearly evident: the former involves a *retention* (or even enhancement) in the extent of bond ionicity as r_{M-A} increases, whereas the latter exhibits an *attenuation* of the degree of metal−adsorbate charge polarization under these conditions.

This adsorbate distinction is depicted in simple energetic terms in Figure 6, which shows adsorbate valence levels in relation to the metal Fermi level, the latter corresponding to an energy Φ_M below the vacuum level, where Φ_M is the metal work function. While the diagram is simplistic, ignoring (among other things) adsorbate level broadening/splitting due to surface−chemisorbate interactions,[36] it provides a qualitative indication regarding the direction of electron polarization from the adsorbate orbital energies in relation to the Fermi level.

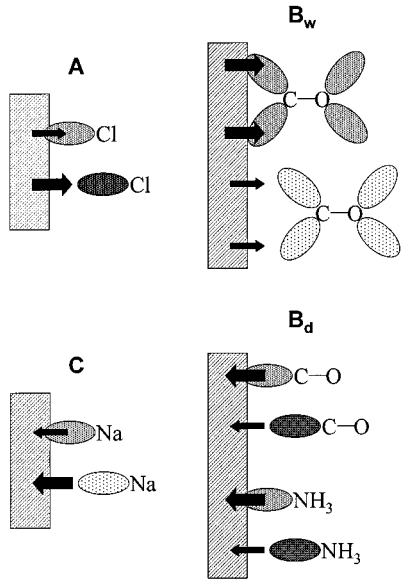

Figure 5. Schematic nature of metal−chemisorbate charge polarization for bonding classifications considered here, as exemplified by orbital interactions for Cl, Na, CO, and NH_3 (see text).

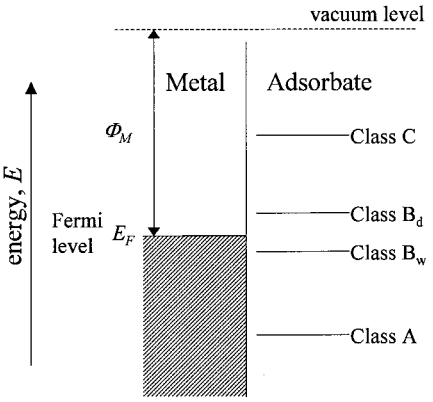

Figure 6. Schematic energy-level plot for metal−adsorbate classification considered here.

Consequences for Field-Dependent Binding Energy and Stark-Tuning Behavior. An important feature of the adsorbate bonding classification just described is that the magnitude and even sign of μ_S and μ_D is sensitive to the applied field as well as the nature of the adsorbate (along with the metal surface and binding-site geometry). In general, applying more negative fields (equivalent to lower electrode potentials) encourages metal-to-adsorbate charge transfer, with the opposite being the case at more positive fields. These trends can be couched in energetic terms, as in Figure 6, by noting that adjusting the electrode potential to more negative values corresponds to lower metal work functions, Φ_M, thereby increasing the E_F-E_A, and decreasing the E_F-E_C, energy separation, where E_A and E_C refer to the adsorbate valence energy levels. Consequently, as we have already seen, one expects ultimately a transition from Class A to B and even C behavior at progressively less negative/more positive fields, depending on the "intrinsic" charge polarization in the surface−adsorbate system (as given by the μ_S/μ_D values at $F = 0$) together with the field sensitivity as determined by the metal−adsorbate polarizability.

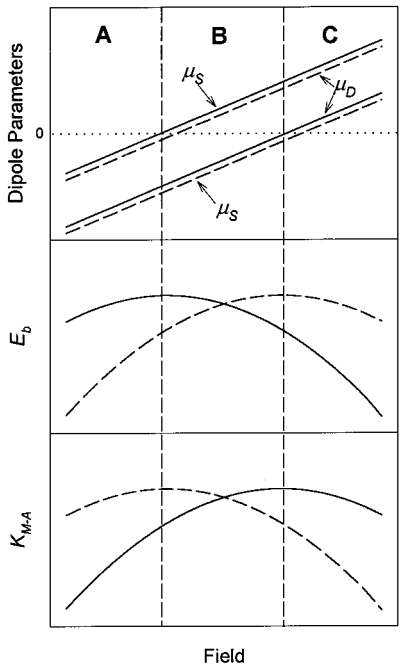

Figure 7. Top segment: Schematic dependence of static (μ_S) and dynamic (μ_D) dipole moments on the applied field, showing field-induced transition expected for Class $A/B_d/C$ and Class $A/B_w/C$ metal−adsorbate bonds (solid and dashed lines, respectively). Middle segment: Corresponding schematic plots of metal−adsorbate binding energy versus field. (Note that increasing bond strength corresponds to lower, i.e., more negative, E_b values.) Bottom segment: Corresponding schematic plots of metal−adsorbate stretching force constant versus field (see text).

This general situation is summarized schematically in the top segment of Figure 7. The most common circumstance is depicted in the upper and lower solid traces, referring to μ_S-F and μ_D-F plots, respectively. (Note that the relative slopes, other than sign, of these plots as shown schematically here have no significance since μ_S and μ_D have different units.) Admittedly, the majority of actual adsorbate systems included in Figure 1 remain in the Class A category throughout the range of fields shown, although, as mentioned above, iodine undergoes a transition to B_d behavior at positive F values. The dashed lines in the top portion of Figure 7 denote the alternative possibility, exemplified here by hollow-site CO (Figure 1), where the application of progressively more positive fields leads instead to a Class A/B_w transition, i.e., μ_D switches sign prior to μ_S.

The middle portion of Figure 7 shows the schematic dependence of E_b versus F expected from eq 2 for the Class $A/B_d/C$ and Class $A/B_w/C$ transitions, shown again as solid and dashed traces, respectively. Note that the binding energy, $-E_b$, is weakest where $\mu_S = 0$, so that the E_b-F plots exhibit a maximum at this point. Finally, the bottom segment of Figure 7 shows the corresponding dependence of the metal−adsorbate force constant, K_{M-A}, upon the field as anticipated from eq 5 in the case where the a_D term can be neglected (this restriction is relaxed below). Given that the anharmonicity term G is uniformly negative (vide infra), the point where $\mu_D = 0$ will correspond to a maximum in the $K_{M-A}-F$ plot.

Inspection of Figure 7 shows that one can, broadly speaking, distinguish between two types of $K_{M-A}-F$ in relation to E_b-F behavior. The first variant, expected for Class A adsorbates,

(36) For example, see (a) Masel, R. I. *Principles of Adsorption and Reaction on Solid Surfaces*; Wiley: New York, 1996; Chapter 3. (b) Hammer, B.; Nørskov, J. K. *Adv. Catal.* **2000**, *45*, 71.

features K_{M-A} values and hence vibrational frequencies, ν_{M-A}, that increase toward less negative/more positive fields. Perhaps surprisingly, however, the E_b-F slopes are also positive under these conditions, i.e., the metal−adsorbate bond becomes *weaker* even though the PES well is progressively stiffer, i.e., K_{M-A} is larger (Figure 7). (Admittedly, the sign of the E_b-F dependence for adsorbates such as chlorine is reversed if E_b refers instead to an ionic, rather than uncharged, bulk-phase reference state.[26,37]) Nevertheless, the lack of a simple correlation between the well *depth* and *stiffness*, as reflected in the field-dependent E_b and K_{M-A} values, is commonly predicted.[37,38] As expected, Class C adsorbates exhibit similar behavior to Class A systems, except that the signs of the E_b-F and $K_{M-A}-F$ slopes are both reversed. In both cases, this arises simply from the occurrence of μ_S and μ_D values having the *same sign*.

Figure 7 also shows that class B adsorbates exhibit distinctly different characteristics resulting from the *opposite* signs of μ_S and μ_D. As a consequence, the field-dependent bonding energies and vibrational frequencies now "correlate", at least qualitatively, in that $-E_b$ increases/decreases along with K_{M-A} as a function of F, the sign of these changes depending on whether the adsorbate classification is B_d or B_w. In this case, then, the field-induced changes in the surface bond energy correlate with the bond stiffness, in contrast to the "anticorrelation" seen with Class A and C adsorbates.[38] However, even for class B systems, the F-dependent *functionality* of $-E_b$ does not correlate with that of K_{M-A} since the anticipated nonlinearity in these plots lies in opposite directions (Figure 7).

These behavioral differences are also clearly evident in Figures 8 and 9, which show $K_{M-A}-F$ and E_b-F plots, respectively, for the four "representative" adsorbates already considered in Figures 4 and 5: Cl, CO, Na, and NH_3. The solid symbols in Figures 8 and 9 are the $K_{M-A}-F$ and E_b-F plots calculated numerically from DFT, although the shapes of these curves (without the intercepts) can also be obtained from eqs 5 and 4, respectively, with a knowledge of the dipole moment and PES parameters (extracted independently from DFT). Also included (as open symbols) in Figure 8 are $K_{M-A}-F$ plots calculated by omitting the second-order dipole term a_D in eq 5 (referenced for convenience to a far negative or positive field). While inclusion of this term is seen to modify the shape of the $K_{M-A}-F$ plots, by and large the field dependence is controlled primarily by the dynamic dipole moment via the combined $(6G\mu_D/K)$ term in eq 5. For completeness, a summary of the constituent parameters appearing in eq 5 as determined by DFT is given for the four specific systems considered here (at $F = 0$) in Table 3.

Comparison of Pt/Cl and Pt/NH_3 in Figures 8 and 9 is particularly instructive. As expected from the negative μ_D values seen in Figure 4, both these adsorbates exhibit positive Stark-tuning ($K_{M-A}-F$) slopes in Figure 8. This behavior is in accordance with experiment, even though data for the metal−NH_3 stretching vibration are apparently available only on palladium and gold electrodes (Table 4). However, we stress again that the bonding modes of Cl and NH_3 are *entirely different*, involving electron withdrawal (Class A) and donation (Class B_d), respectively, to the metal surface: this is reflected

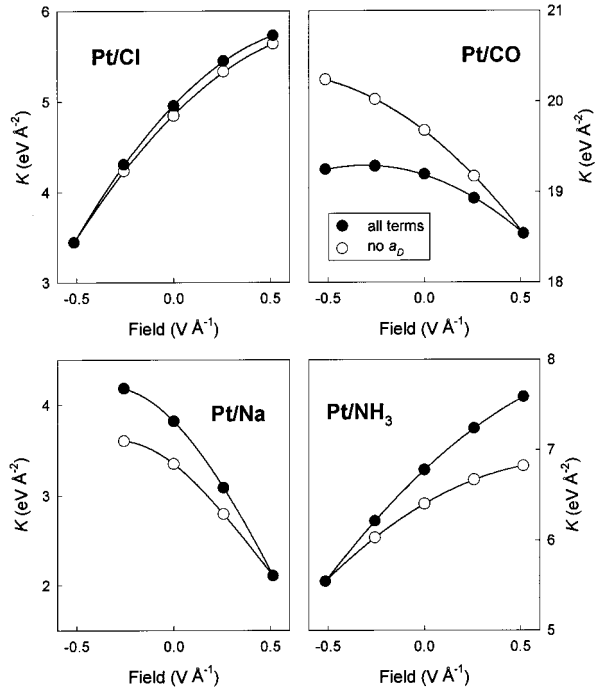

Figure 8. Plots of force constant for Pt(111)−adsorbate stretching vibration versus field as calculated from DFT for hollow-site Cl and Na and atop CO and NH_3, as indicated. Open symbols refer to calculations based on eq 5, omitting the second-order dipole moment term a_D, and referenced to either extreme negative or positive fields (whereas curves coincide with full DFT calculations, shown as solid symbols).

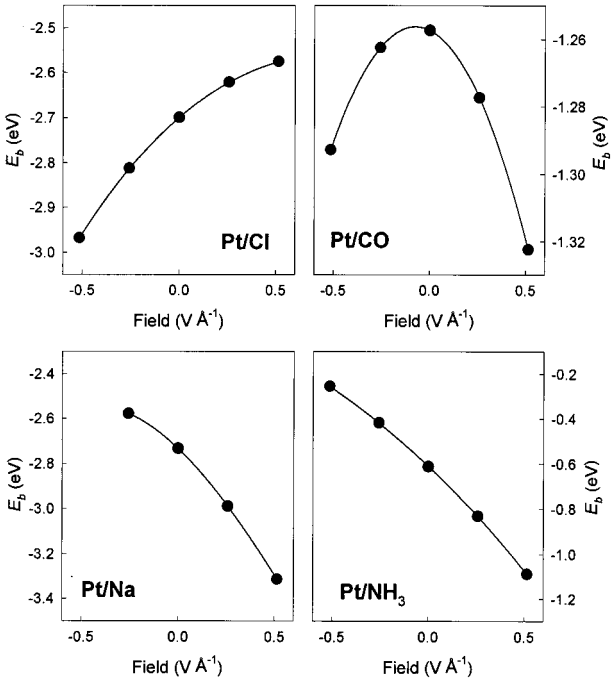

Figure 9. Plots of Pt(111)−adsorbate binding energies versus field as calculated from DFT for the systems considered in Figure 8.

(37) Wasileski, S. A.; Weaver, M. J. *Faraday Discuss.*, in press.
(38) Overall correlations between changes in $-E_b$ and K, i.e., between well depth and well stiffness, are often presumed on simple intuitive grounds. However, the underlying physical reasons for the lack of a general correlation along these lines for field-induced effects, as considered here, are simply understood: $-E_b-F$ behavior is determined by μ_S, whereas the $K-F$ dependence is controlled primarily by μ_D (eqs 2 and 5). Nevertheless, as outlined in ref 10, a general (inverse) correlation between field-dependent K values and the corresponding changes in equilibrium bond lengths, r_{eq}, is indeed predicted, since both parameters are controlled by μ_D. In other words, the F-induced changes in both these parameters (K and r_{eq}) are controlled by the motion of charge as the bond is stretched (the $\mu-r$ slope, i.e., μ_D), whereas the $-E_b-F$ behavior is dependent only on the "absolute" value of the bond polarization at $r = r_{eq}$, i.e., μ_S.

Table 3. Summary of Constituent Stark-tuning Parameters at $F = 0$

bonding parameter	Pt/Cl [a]	Pt/Na [a]	Pt/CO [a]	Pt/NH_3 [a]
G [b] (eV Å^{-3})	−1.75	−1.6	−20.5	−6.6
K [c] (eV Å^{-2})	4.95	3.8	19.2	6.8
μ_D [d] (e$^-$)	−1.0	0.65	0.25	−0.2
$-2a_D$ [e] (e$^-$ Å^{-1})	−0.1	0.65	−0.95	−0.75
$6G\mu_D/K$ [f] (eV V^{-1} Å^{-1})	2.1	−1.65	−1.7	1.15
dK/dF [g] (eV V^{-1} Å^{-1})	2.0	−1.0	−2.6	0.4

[a] Numerical values for each parameter were rounded off to the nearest 0.05, for clarity. [b] Anharmonicity parameter, obtained from fitting the DFT potential-energy surface to eq 4. [c] Harmonic force constant, obtained as in footnote *b*. [d] Dynamic dipole moment, obtained by fitting $\mu-q$ DFT data to eq 1. [e] Second-order dipole derivative, obtained as in footnote *d*, multiplied by −2. [f] Coefficient in eq 5, obtained from constituent parameters as noted above. [g] Overall force constant−field (Stark-tuning) slope, obtained from eq 5 by use of the constituent parameters tabulated above.

Table 4. Representative Experimental Stark-tuning Slopes for Electrode−Chemisorbate Stretching Vibrations

surface	adsorbate	$d\nu_{M-A}/d\phi$ [a] (cm^{-1} V^{-1})	dK_{M-A}/dF [b] (eV V^{-1} Å^{-1})
Pd	Cl	20[c]	5
Au	Cl	35[d]	8
Pt	Cl	∼15[e]	∼4
Pd	N	20[f]	3.5
Pd	NH_3	∼10[f]	∼2
Au	NH_3	30[f]	5
Pt(a)	CO	8[g]	2.5
Ir(a)	CO	7[h]	2.5

[a] Experimental metal−adsorbate frequency−electrode potential slopes, obtained from literature sources indicated, typically for approximate field range −0.3 to 0 V A^{-1}. [b] Metal−adsorbate force constant−field slopes, extracted from $d\nu_{M-A}/d\phi$ data in adjacent column, neglecting anharmonicity, along with ν_{M-A} frequencies evaluated at ca. 0.2−0.4 V vs SCE, as follows (from literature cited for each system): Pd/Cl, 270 cm^{-1}; Au/Cl, 265 cm^{-1}; Pt/Cl, 275 cm^{-1}; Pd/N, 450 cm^{-1}; Pd/NH_3, 440 cm^{-1}; Au/NH_3, 370 cm^{-1}; Pt/CO, 460 cm^{-1}; Ir/CO, 505 cm^{-1}. [c] Reference 13a. [d] Reference 13b. [e] Estimated value. [f] Reference 15c. [g] Reference 14a. [h] Reference 14b.

in the opposite E_b-F dependences for these systems evident in Figure 9. A similar situation pertains to N versus NH_3 adsorption, with positive Stark-tuning slopes being predicted (and measured) in both cases (Table 4) despite the opposite direction of metal−chemisorbate charge polarization.

In contrast, both the Pt/Na and Pt/CO systems exhibit essentially *negative* Stark-tuning slopes (Figure 8): although the former system is immeasurable, the latter prediction is again in accord with experiment (Table 4). While the Pt/CO system is not strictly class B_w except at negative fields (vide supra), the opposite E_b-F slopes seen under these conditions compared to the Pt/Na system (Figure 9) again points to distinct surface-bonding modes (Class B_w versus C) despite the similarity of the Stark-tuning behavior. On the other hand, the negative and positive Stark-tuning slopes obtained for Pt/CO and Pt/Cl (Figure 8), despite the electron-withdrawing nature of both adsorbates as reflected in similarity of their E_b-F dependences for $F < 0$ (Figure 9), provides a clear signal that the mode of surface coordination is fundamentally different. Interestingly, the metal−CO stretching vibrations on noble-metal electrodes constitute, to our knowledge, the only examples of negative Stark-tuning slopes measured up to now.

These and several other pertinent experimental examples for noble-metal electrodes are summarized, both as measured Raman frequency−potential ($\nu_{M-A}-\phi$) and derived $K_{M-A}-F$ slopes, in Table 4. While a rough concordance between the experimental and calculated $K_{M-A}-F$ slopes (Figure 8) is evident, a more quantitative agreement is neither expected nor obtained, partly since the influence of double-layer solvation is neglected in the present illustrative DFT calculations.

Concluding Remarks

The present surface dipole analysis and accompanying DFT calculations furnish an important clarification of the vibrational Stark-tuning behavior observed for electrode−chemisorbate bonds in relation to adsorbate binding energetics in terms of the fundamental nature of the surface coordination. Although the magnitude of μ_D, determining the Stark-tuning slope (dK_{M-A}/dF), is related only indirectly to the direction of metal−adsorbate charge transfer (i.e., μ_S), which controls dE_b/dF, the qualitative sign of these fundamental quantities can be predicted on the basis of our adsorbate bonding classification. At least for a range of applied fields mild enough not to change the "intrinsic" adsorbate bonding character, both anionic and electron-donating molecular adsorbates yield negative μ_D values and hence positive $K_{M-A}-F$ slopes; the opposite is true for the cationic and electron-withdrawing molecular adsorbates. However, the opposite signs of μ_S expected for anionic and electron-donating "covalent" molecular adsorbates mean that their E_b-F dependences are qualitatively different, with a similar situation applying to cationic and other electron-withdrawing systems. Contrary to conventional wisdom, then, the sign (and magnitude) of the Stark-tuning slope does not necessarily provide straightforward information on the direction of charge polarization but reflects another aspect of surface coordination, specifically ionic versus dative covalent bonding.

Consequently, the electrode−chemisorbate classification scheme presented here, deduced on the basis of the field-dependent μ_S versus μ_D behavior, provides an invaluable framework by which such Stark-tuning behavior *combined* with binding energy−field data obtained separately can yield detailed insight into the quantum-chemical nature of the field-dependent surface bond. Although complete experimental data along these lines are available only for a few systems, a potentially powerful approach for exploring such issues involves harnessing DFT calculations along with vibrational spectral information. Aside from the opportunities to test the ability of the computational models to describe actual electrochemical interfaces, the DFT calculations can, in return, provide predictive estimates of parameters (such as field-dependent bond geometries and energies) which are often inaccessible to experiment, especially for electrochemical systems. The value of such combined computational−experimental approaches should grow apace as more sophisticated DFT approaches, especially those based on periodic slabs, become commonplace in modeling variable-potential electrochemical interfaces.

Finally, while the present discussion has centered on the vibrational properties of the metal−chemisorbate bond itself, a corresponding analysis of *intramolecular* vibrational Stark behavior in terms of dynamical bond polarization can also be undertaken, although the link to binding energies is necessarily more tenuous. Given the greater abundance of such intramolecular Stark behavior for electrochemical systems, such analyses are of broad-based interest, especially in view of the ability of DFT calculations to explore the quantum-chemical consequences of surface binding on the internal adsorbate vibrational properties.[9]

Acknowledgment. S.A.W. is grateful to Eastman Chemical Company for an American Chemical Society Analytical Division summer fellowship and to Procter and Gamble Corporation for a Purdue University graduate fellowship. This work is also supported by the National Science Foundation (Analytical and Surface Chemistry Program) and the Petroleum Research Fund (to M.J.W.) and by a fellowship of the Royal Netherlands Academy of Arts and Sciences (to M.T.M.K.).

JA012200W